Journal of CO2 Utilization 75 (2023) 102582

Contents lists available at ScienceDirect

Journal of CO2 Utilization

journal homepage: www.elsevier.com/locate/jcou

Decisive role of Cu/Co interfaces in copper cobaltite derivatives for high performance CO_2 methanation catalyst

Gábor Varga [a,*,1], Imre Szenti [b], János Kiss [b,c], Kornélia Baán [b], Gyula Halasi [b,d], László Óvári [c,d], Ákos Szamosvölgyi [b], Róbert Mucsi [b], Erzsébet Dodony [e], Zsolt Fogarassy [e], Béla Pécz [e], Luca Olivi [f], András Sápi [b,*], Ákos Kukovecz [b], Zoltán Kónya [b,c]

[a] Department of Physical Chemistry and Materials Science, University of Szeged, Rerrich Béla tér 1, Szeged H-6720, Hungary
[b] University of Szeged, Interdisciplinary Excellence Centre, Department of Applied and Environmental Chemistry, Rerrich Béla tér 1, H-6720 Szeged, Hungary
[c] MTA-SZTE Reaction Kinetics and Surface Chemistry Research Group, Rerrich Béla tér 1, Szeged H-6720, Hungary
[d] ELI-ALPS, ELI-HU Non-Profit Ltd., Wolfgang Sandner utca 3, H-6728 Szeged, Hungary
[e] Centre for Energy Research, Institute for Technical Physics and Materials Science, Konkoly-Thege M. út 29-33, Budapest 1121, Hungary
[f] Elettra Sincrotrone Trieste, Strada Statale 14-km, in AREA Science Park, 34149 Basovizza, Italy

ARTICLE INFO

Keywords:
Spinel precursors
CuCo bimetallic catalysis
Co/CoO/Cu interface
Efficient CO_2 methanation
Structural aspects
Active carbon hydrogenation

ABSTRACT

Thermo-catalytic bio-SNG (CH_4) production is one of the useful tools for converting waste to gaseous fuels through CO_2 conversion. To abundant properly, however, efficient, robust and cost-effective catalysts would be required. Bimetallic systems based on transition metals seem to be promising candidates for this task. The CoCu bimetallic system with in-situ generated interfaces was synthesized and used as a catalyst for CO_2 methanation. The in-depth analysis of the structure-activity-selectivity relationships involving XRD, (NAP-)XPS, EXAFS and TEM-EDX revealed that the co-existence of Co^0, CoO, and Cu^0 in the proper distribution on the surface can ensure the selective production of methane. To fine-tune the surface composition of the bimetallic systems, a systematic alteration of the Cu:Co ratio in the precursor spinel structures must be performed. $Cu_{0.4}Co_{2.6}O_4$ derivative, stabilizing subsurface Cu(I)–O specimen, showed the best performance with high activity (12,800 nmol g^{-1} s^{-1}) and a remarkable selectivity of 65–85% for methane in a wide temperature range (250–425 °C). In studying the mechanistic aspects of methanation, it has been shown that the hydrogenation of active carbon at the surface or below the surface is the key step for the production of methane. So far, this cobalt-catalyzed sub-step has been proposed in catalytic Fischer-Tropsch syntheses.

1. Introduction

Bimetallic structures with intimate metal-promoter interactions are well-known advanced multifunctional materials [1]. Their applications range from groundwater remediation [2], ocean fertilization [3] and bio-nano applications [4,5] to heterogeneous catalysis [6–8] due to their higher efficiency compared to monometallic systems, which is closely related to the promoter effect [9]. Based on this phenomenon, considerable progress has been achieved nowadays in the thermo-catalytic valorization of CO and CO_2 [10], especially in their hydrogenation to methane [11]. These processes are becoming increasingly important as the market for SNG and bio-SNG, which can also contribute to climate protection, is growing strongly [12]. A number of active catalysts based on the combination of different noble and transition metals and their oxides such as Cu, Pt, Rh, Ce, Co, Fe, Ni, Zn or Mn *etc*. have already been introduced [13–17]. As far as green chemical approaches are concerned, the focus has recently shifted to the application of the more suitable, non-expensive and non-toxic transition metal compounds [18,19]. As of yet, the issue of replacing the most active supported Rh and Ru catalysts has not been resolved, especially in industry [20]. This could change with the development of efficient bimetallic systems.

However, when using bimetallic systems, it remains a challenge to properly understand the structure-composition-performance relationships and consequently to rationally design the catalyst formulation [21]. Moreover, in most cases, the use of easy-to-regulate impregnation methods that can provide well-ordered active surfaces is not an option,

* Corresponding authors.
E-mail addresses: gabor.varga5@chem.u-szeged.hu (G. Varga), sapia@chem.u-szeged.hu (A. Sápi).
[1] Present address: Australian Institute for Bioengineering and Nanotechnology, The University of Queensland, Brisbane, QLD 4072, Australia.

https://doi.org/10.1016/j.jcou.2023.102582
Received 12 June 2023; Received in revised form 13 August 2023; Accepted 28 August 2023
Available online 30 August 2023

as they cannot be used to ensure the necessary tight metal-promoter interactions [22]. For this purpose, simple co-precipitation or the well-known sol-gel methods have found to be useful. With the introduction of these methods, the surface composition and the (co-)existence of the active surface specimens have become variables that depend on the reaction conditions of the synthesis procedures and the molar ratios of the precursors [23]. Spinel oxide structures have often been used as catalyst precursors for the preparation of these bimetallic catalysts [24]. Previously, it has been reported that the catalytic performance of these systems –prepared from spinel oxides – can be fine-tuned by altering the preparation method of the precursor or the molar ratio of metal ions in the oxide phase [25].

Both copper- and cobalt-based catalytic systems appear to be promising candidates to play a key role in the commercialization of CO_2 [26–30]. However, it has been shown that not only the catalytic activity but also the selectivity of these composites strongly correlates with the formation, co-existence and transformation of certain crystalline phases ($CuO \rightarrow Cu_2O \rightarrow Cu$ [31]; $Co_3O_4 \rightarrow CoO \rightarrow Co$) [32]. In addition, the use of promoters or carriers can also alter which phase appears to be active depending on the quality of the second component [30]. Weckhuysen and co-workers have recently shown that, contrary to the paradigm of metallic cobalt as the only active phase, an efficient CoO-based catalyst can be synthesized if one finds the appropriate support or promoter, in this case TiO_2 [33]. It is noteworthy that all other catalysts studied, except for the aforementioned CoO/TiO_2, work more efficiently when they contain metallic cobalt. Besides, Luo and co-workers have recently shown that cobalt/cobalt oxide composite catalysts can play the main role in CO_2 hydrogenation without using any promoters or supports. However, this requires fine-tuning of the surface composition. They found that this fine-tuning can be achieved if spinel oxides (Co_3O_{4-x}) are used as precursors [32].

Although CuCo alloys and bimetallic Cu-Co composites have shown to be active and selective catalysts for promoting CO hydrogenations [34–36] as well as low-temperature CO_2-to-alcohol conversions in the slurry phase [37–40], few studies have addressed heterogeneous catalytic CO_2 conversions in the gas phase [41,42]. Moreover, these studies have reported the negligible activity of copper-cobalt alloys even under relatively high gas pressure conditions. But in these cases, the molar ratios of the active species in the precursors were approximately one. However, from the much better studied hydrogenations noticed above, it appears that the catalytic performance of CuCo alloys can be readily altered by changing their surface composition. Recently, Zhao and co-workers determined the optimal surface composition and metal distribution to maximize the alcohol yield in a slurry-phase CO_2 hydrogenation [39]. They found that the enrichment of copper centers on the surface combined with moderate segregation resulted in maximum alcohol yield. However, there is no information on how to tune the surface properties of CuCo alloys to achieve an efficient catalyst for CO_2 hydrogenation. Furthermore, it is also not clarified whether the use of spinel oxides as precursors of the actual catalyst can produce what kind of catalytic surface and whether there is a possibility to control their composition.

These caveats motivated us to find the optimal surface composition of a Cu-Co(CoO_x) bimetallic system to achieve the maximum CH_4 yield in a heterogeneous catalytic CO_2 hydrogenation in the gas phase. To modify the surface composition of the catalyst candidates, the initial molar ratio of the cations is systematically changed during the synthesis of $Cu_xCo_{3-x}O_4$. By combining different surface-sensitive (DRIFTS, XPS, TEM-EDX) and bulk-sensitive (Raman, XRD, EXAFS) as well as analytical (ICP-MS) methods, a well-established relationship between the structure of the precursor spinels, which is dictated by the initial molar ratio of the cations, and the surface composition of the catalysts and their catalytic performance can be identified.

2. Experimental part

2.1. Materials

$Co(NO_3)_2 \times 6H_2O$ (≥98%), $Cu(NO_3)_2 \times 6H_2O$ (99%), citric acid (99%) were purchased from Sigma-Aldrich, while the applied gases (H_2, CO_2, He; 99.99%) were purchased from Messer Hungary as compressed gases. All chemicals were used as received without further purification.

2.2. Catalyst preparation, activation and regeneration

The $M_xCo_{3-x}O_4$ (M = Cu, Co) spinel oxides were synthesized by a simple sol-gel method. In a typical procedure, the starting materials $Co(NO_3)_2 \times 6H_2O$ (c = 0.2–0.29 M) and $Cu(NO_3)_2 \times 6H_2O$ (c = 0.01–0.1 M) were dissolved separately in distilled water of 25 ml. They were then mixed for 10 min and citric acid (c = 0.44 M) was added to the solution at room temperature with constant magnetic stirring. The resulting mixed solution was stirred vigorously at 80 °C for 2 h until the gel was formed. It was then heated at 110 °C until a powder was formed. The precursor thus prepared was then calcined at 550 °C for 5 h with a ramp of 5 °C/min to obtain the final products. The as-prepared spinels are referred to in the text as s-Co_3, s-$Cu_{0.1}Co_{2.9}$, s-$Cu_{0.4}Co_{2.6}$ and s-$CuCo_2$ (Table 1), where "s" stands for spinel and the initial molar ratios of copper-to-cobalt are given in the abbreviations.

Prior to the catalytic experiments, the as-prepared catalysts were activated in the reaction chamber. First, the freshly prepared pellets were 30-minute-long oxidized in an O_2 atmosphere at 300 °C which was followed by the second, reductive step in which the pellets were reduced in H_2 at 300 °C for 60 min. The pre-treatment conditions were the same for all other characterization measurements.

After using s-$Cu_{0.4}Co_{2.6}$ at 300 °C, the spent sample was regenerated based on the literature processes [43]. The obtained residue was re-oxidized in O_2 during a 180-minute-long treatment at 400 °C, which rearranged the reordered spinel structure. Subsequently, the regenerated sample was reused under the same activation and reaction conditions as described above.

2.3. Catalytic measurements

The CO_2 hydrogenation reactions were performed at a pressure of 1 atm in a continuous-flow fixed-bed reactor (8 mm *i.d.*) combined with a thermocouple for accurate control of the reactor temperature. The reactor typically contained 200 mg of slightly compressed pellets as catalyst and the dead volume of the reactor was filled with quartz. In the reaction gas mixture, the molar ratio of carbon dioxide to hydrogen was 1:4. The gas mixture was introduced into the reactor at a total flow rate of 50 ml/min. To follow the reactions, an Agilent 4890 gas chromatograph was used, equipped with Equity-1 capillary and Porapak QS packed columns, as well as thermal conductivity and flame ionization detectors.

2.4. Characterization methods

Powder X-ray diffractograms (XRD) were recorded in the range 2θ = 5–80° with a Rigaku Miniflex II instrument at a scanning speed of $4^\circ min^{-1}$ using Cu Kα radiation (λ = 0.15418 nm) at 40 kV, 30 mA. The characteristic reflections were identified based on the database JCPDS-

Table 1
As-prepared structures with their nominal Cu:Co ratios and labels.

As-prepared composite	Nominal Cu:Co ratio	Labeled as
Co_3O_4	—	s-Co_3
$Cu_{0.1}Co_{2.9}O_4$	0.1:2.9	s-$Cu_{0.1}Co_{2.9}$
$Cu_{0.4}Co_{2.6}O_4$	0.4:2.6	s-$Cu_{0.4}Co_{2.6}$
$CuCo_2O_4$	1:2	s-$CuCo_2$

ICDD (Joint Committee of Powder Diffraction Standards- International Centre for Diffraction Data).

An Agilent 7900 inductively coupled plasma mass spectroscope (ICP-MS) was used to determine the actual molar ratios of the metallic components in the spinel oxides. The Aristar® multi-element calibration standard was used for quantitative analysis.

A gas adsorption analyzer (Quantachrome NOVA 3000e) at a liquid nitrogen temperature of −196 °C was used to determine the specific surface area (S_{BET}) of the prepared spinels. Prior to the measurements, each sample was degassed at 250 °C for 2 h under vacuum. The evaluation of the results was based on the Brunauer-Emmett-Teller equation (BET).

The temperature programmed reduction (TPR) measurements were performed in a BELCAT-A apparatus using an externally heated reactor (quartz tube with an outer diameter of 9 mm). Prior to the measurements, the catalyst samples were treated in oxygen at 200 °C for 30 min. Afterwards, the samples were cooled down to room temperature in flowing N_2. Then the oxidized samples were flushed with N_2 containing 10% H_2 for 30 min, flushed with N_2 for 15 min and the reactor was heated linearly from 50 °C to 800 °C at a rate of 10 °C/minute. H_2 consumption was monitored with a thermal conductivity detector (TCD). The flow rate was 50 ml/min in all cases.

The CO_2-temperature-programmed desorption (CO_2-TPD) was performed in a BELCAT-A apparatus using an externally heated reactor (quartz tube with 9 mm outer diameter). Prior to the measurements, the spinels were pre-heated as described above. Thereafter, the samples were cooled in flowing He to 50 °C and equilibrated for 15 min. The samples were flushed with CO_2 for 30 min and then flushed with He for 15 min at 50 °C. After that, the reactor was heated linearly at a ramp of 10 °C min^{-1} up to 650 °C. The CO_2 consumption was measured by a thermal conductivity detector (TCD).

Raman spectra were recorded using a Bruker Senterra II Raman microscope. Spectra were recorded using a light source of 532 nm wavelength and 12.5 mW laser power. For each sample, 32 spectra were collected and averaged with an exposition time of 6 s.

Co K-edge and Cu K-edge X-ray absorption spectroscopy (XAS) measurements were performed at room temperature on the XAFS beamline of the ELETTRA synchrotron in Trieste (Italy). Prior to the measurements, the powder samples were pelletized with boron nitride. The XAS spectra were recorded in the energy range of 6.5–8.9 keV for the Co K edge and 8.6–9.9 keV for the Cu K edge, respectively, in transmission mode. A Si (111) double crystal monochromator was used during the measurements. The software package "EXAFSPAK" was used to analyze the collected data. The data range of 3.0–13.0 Å for the k^3 Fourier transform (FT) was used, while the range of 1.2–4.5 Å was used for the interpretation of the X-ray absorption fine structure (EXAFS) oscillation.

A Kratos XSAM 800 instrument was operated with a Mg Kα X-ray source of 120 W power (12 kV) to record *ex-situ* X-ray photoelectron spectra (XPS). The pre-treatment and reaction were carried out in the modified pre-chamber of the instrument, where the samples could be treated without exposing them to atmospheric moisture and oxygen. During the measurement, the chamber pressure was $\sim 2 \times 10^{-8}$ mbar. The high-resolution spectra were recorded with a pass energy of 20 eV and a step size of 0.1 eV. Data analysis was performed with CasaXPS software version 2.3.25 [44].

Near ambient pressure X-ray photoelectron spectroscopy (NAP-XPS) and Auger spectroscopy (AES) measurements were performed with the SPECS system at Charles University in Prague. A monochromatic Al Kα X-ray source was used for excitation and a hemispherical PHOIBOS 150 energy analyzer with a differentially pumped electrostatic pre-lens system was used for spectrum acquisition. The spectra presented here were obtained with a constant pass energy of 20 eV, while the background pressure in the analyzer was $\sim 5 \times 10^{-9}$ mbar. All experiments were performed in the mbar range. The binding and kinetic energies were referenced to the Fermi level, and CasaXPS version 2.3.25 was used for data analysis [44].

Transmission electron microscopy (TEM) images of the pre-treated and spent catalysts were taken with a Philips CM20 instrument at an accelerating voltage of 200 kV, and a Cs-corrected scanning/transmission electron microscope from Themis was used. The TEM-EDX mapping was monitored by the Super-X detectors of the Themis instrument at 200 kV. Morphology of each sample were characterized with using a FEI TECNAI G^2 20 X-Twin high-resolution transmission electron microscope (equipped with electron diffraction) operating at an accelerating voltage of 200 keV.

3. Results and discussion

3.1. Characterization of the as-prepared oxides

Three catalyst candidates with different initial molar ratios of metal ions and a pure Co_3O_4 structure for comparison were synthesized and characterized by fundamental techniques (Fig. 1, Table S1). The XRD patterns of the as-prepared copper-containing cobaltites (Fig. 1 (A)) are analogous to those of a phase-pure cubic spinel structure identified in the JCPDS database (PDF#23–1237). The ICP-MS analysis verified that the molar ratios of the cations are almost identical to the initial ratios (Table S1), supporting the fact that the synthesis of the spinel structures were successful [45]. Each solidified product has a semi-regular round cubic shape (Fig. 1 (F)) and a relatively low specific surface area (Table S1; ~20 m^2/g) except for s-Co_3 owning 110 m^2/g specific surface area.

Raman spectroscopy is a suitable method to distinguish the structural polymorphs of spinels from each other (Fig. 2). Co_3O_4 possesses a normal spinel structure with Co^{2+} ions in the tetrahedral positions and Co^{3+} in the octahedral positions [46]. As a result, the fingerprint-like Raman bands (A_g^1; F_{2g}^2; F_{2g}^1; E_g; T_{2g}) appear at band positions 690, 620, 521, 481 and 194 cm^{-1} [47,48]. While Raman bands in the higher energy range (> 600 cm^{-1}) are sensitive to changes in the octahedral positions, those that can be found in the lower energy range (< 600 cm^{-1}) are markers for changes in tetrahedral positions. Because of theoretical reasons, copper(II) cations can occupy both coordinatively different positions in the spinel structures, which can even induce the transformation of the normal spinel structure into an inverse or mixed spinel structure. There is a reason that copper-containing spinels usually have inverse or mixed spinel structures. Given different values of the crystal field stabilization energy (CFSE) of the copper and cobalt cations, mixed spinel structures are most likely to form with copper and cobalt cations in both positions [49]. In agreement with this suggestion and with literature data, the characteristic bands of the copper-cobaltites shifted significantly to the lower energy range, indicating the development of mixed spinel structures. However, no significant shift was observed when the original Co:Cu ratio of 2.6:0.4 was used. This should be considered as a marker for the existence of an almost normal spinel structure with a slight structural distortion. This distortion is probably related to the Jahn-Teller torsion.

3.2. Catalytic performances of the activated spinels

With the phase-pure spinel oxides in our hands, their catalytic performances were tested in a CO_2 methanation reaction (Figs. 3, S1, S2; Table S2). After reductive and oxidative pre-treatment of the pure oxides, which was carried out in the reaction chamber, all activated samples promoted reductive conversion of CO_2. However, the catalytic capabilities of the active samples differed significantly from each other, and the observed changes in catalytic behavior can be readily related to the differences in the initialized cation ratios. First of all, it can be observed that the values of the onset temperature (Fig. S1) are particularly dependent on the copper-cobalt ratio (Fig. 3 (B)). By inserting copper ions into the spinel structure, lower initial temperatures could be

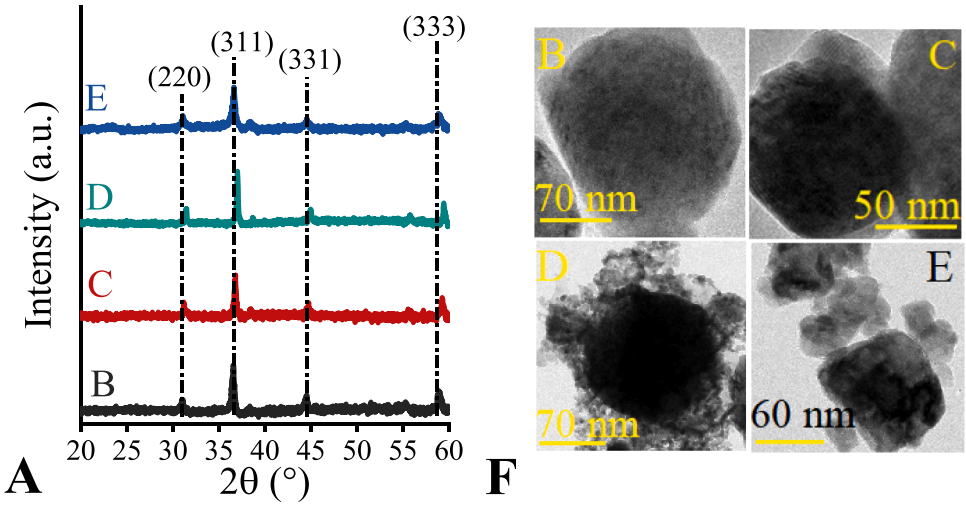

Fig. 1. XRD patterns (A) and TEM images (F) of the as-prepared s-Co_3 (B), s-$Cu_{0.1}Co_{2.9}$ (C), s-$Cu_{0.4}Co_{2.6}$ (D) and s-$CuCo_2$ (E).

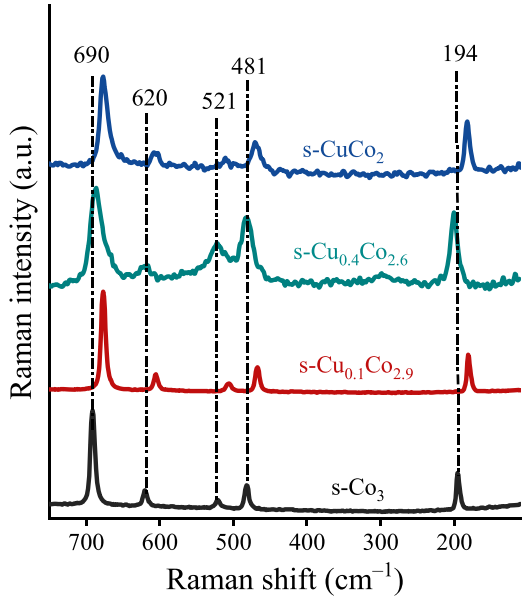

Fig. 2. Raman spectra of the as-prepared s-Co_3 (black), s-$Cu_{0.1}Co_{2.9}$ (wine-colored), s-$Cu_{0.4}Co_{2.6}$ (cyan) and s-$CuCo_2$ (blue).

obtained, but the temperature decrease is not linear with the introduced copper values. The s-$Cu_{0.4}Co_{2.6}$ derivative – with a copper-to-cobalt ratio of 0.15 – has the most reduced initial temperature (250 °C) and selectively produces methane at this temperature (Table S2). Moreover, the maxima of CO_2 consumption rates of the different bimetallic systems were in the order of s-Co_3 < s-$Cu_{0.1}Co_{2.9}$ < s-$CuCo_2$ < s-$Cu_{0.4}Co_{2.6}$ in the temperature range of 250–450 °C. This order also corresponds to the onset temperatures and methane selectivities, respectively. When the reaction temperature was increased from 300 °C to 550 °C, the CO_2 consumptions should have increased due to the lower thermodynamic limitation, while methane selectivity decreased in agreement with previously reported results [23]. And this occurred in the temperature range below 450 °C. In contrast, when the temperature was further increased, there was a significant decrease in the consumption rates, except for s-Co_3, in addition to the complete CO selectivity. This can be explained by the dynamic change of the active surface as a function of the reaction temperature or by the appearance of the amorphous carbon layer that can cover the active sites. See the last chapter for a more detailed explanation. However, the experienced differences in the activity and selectivity of the spinel derivatives compared to each other remain. For example, the s-$Cu_{0.4}Co_{2.6}$ derivative still produced significant amounts of methane even at 425 °C, in contrast to the other derivatives, which yielded methane up to 350–375 °C. Therefore, it can be assumed that the catalytic ability of the spinel derivatives depends on the original composition of the samples.

When the consumption rates were determined as a function of reaction time to determine the robustness of the catalysts by maintaining the temperature at 300 or 550 °C (Fig. 4, Table S3), both the selectivities and the remarkable activities of the spinel derivatives were maintained. It became clear that the s-$Cu_{0.4}Co_{2.6}$ derivative is able to maintain its methane selectivity upon catalytic hydrogenation at 300 °C even for 6 h. It can be concluded that copper-containing bimetallic systems act as robust catalysts for CO_2 methanation. Moreover, spinel oxide structures with detectable amorphization can be reconstructed by a simple regeneration process, which was verified by XRD (Fig. S3). However, the amorphization of the original structure does not affect the catalytic ability of the catalysts (Fig. 4, Table S2). The catalytic markers obtained with the reconstructed oxides were similar to those collected when using the as-prepared structures.

3.3. Structural aspects of the activated spinels

In order to understand the reason for the observed differences in catalytic capabilities, the structural aspects of the pre-treated and spent catalysts were investigated by a systematic combination of XRD, TPR, EXAFS, XPS, NAP-XPS and TEM-EDS measurements.

For all copper-containing spinel structures, the XRD patterns (Figs. 5 (A), S4) of both the pre-treated and spent catalysts can be assigned to the Bragg reflections of a metallic CuCo alloy solidified in a face-centered cubic (FCC) crystal phase (PDF#15–806). Based on the TPR measurements (Fig. 5 (B)), complete reduction of each sample can indeed be expected, considering that each copper-containing spinel can be completely reduced at maximum 260 °C in H_2. Noticeably, significant baseline shifts of diffractograms were also observed in all cases, probably indicating the presence of an amorphous phase. No differences were observed between the XRD patterns of the derivatives that would indicate phase separation of the copper and cobalt components or significant distortion of the FCC structure.

To determine whether the structures are exactly the same at different copper-content, Cu K-edge (Figs. 6, S5) and Co K-edge (Figs. 7, S5) XAS measurements (Table S4) were introduced. The first three coordination spheres of the cations in the as-prepared (black colored in all spectra/curves) structures can be readily described as cationic centers in spinel oxides that strengthened that no other phase in the solid catalysts. For

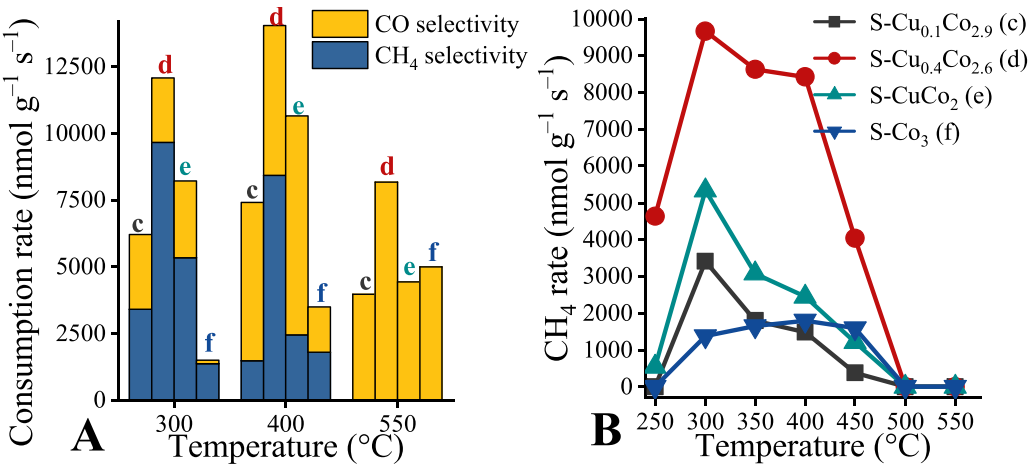

Fig. 3. Consumption rate (A) and CH_4 yield (B) of catalytic CO_2 methanation reactions promoted by activated s-$Cu_{0.1}Co_{2.9}$ (c), s-$Cu_{0.4}Co_{2.6}$ (d), s-$CuCo_2$ (e) and s-Co_3 (f) derivatives on different temperatures.

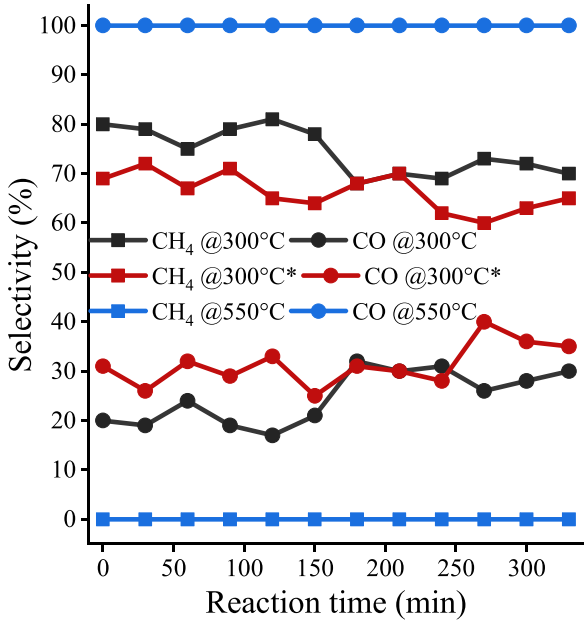

Fig. 4. Robustness test of the catalysts. CH_4/CO selectivity of catalytic CO_2 methanation reactions promoted by activated s-$Cu_{0.4}Co_{2.6}$ derivative and regenerated-activated s-$Cu_{0.4}Co_{2.6}$ derivative (*) at 300 and 550 °C. (Test reactions were carried out continuously after the temperature-dependent tests.).

the fitting of the EXAFS spectra of the as-prepared samples, the co-existence of tetrahedral coordinated Cu(II)/Co(II) centers and Cu(II)/Co(III) centers in the octahedral positions had to be considered [50]. Noticeably, for fitting the EXAFS spectrum of s-$Cu_{0.4}Co_{2.6}$, tetrahedral coordinated Cu(II) centers are much more represented than any other case. This is made abundantly clear when taking into account the reduced coordination number (4.2) and reduced interatomic distance (1.44 Å) that were associated with the copper-oxygen distance in the first coordination sphere.

However, the EXAFS refinement results also showed that the spinel oxides undergo only a partial reduction due to the pre-treatment (wine-colored ones). In each sample, a considerable amount of CoO retained after the pre-treatment [51], so concerned, that no other specimen can be considered for describing the coordination sphere of cobalt in the case of s-$Cu_{0.1}Co_{2.9}$. In the other two samples, both CoO and metallic cobalt co-exist, but CoO phases are in access. This is based not only on the EXAFS refinements but also on the XANES spectra providing well-known spectral shapes that are almost identical to those of the CoO in all cases [52]. Furthermore, the edge positions also indicated the co-existence of the CoO specimen [53]. As for the copper coordination spheres, the characteristic interatomic distances of Cu(II)–O disappear completely and only the interatomic distance between the metallic centers remains. As a result, the EXAFS region can be fitted with the known EXAFS parameters of metallic components with face-centered cubic (FCC) structure [54]. However, there is one exception to this observation, namely s-$Cu_{0.4}Co_{2.6}$. To describe the EXAFS oscillation of its EXAFS spectrum, an interatomic distance between Cu(I)(cuprous)–O of 1.64 Å must be included in the model [55]. This distance is shorter than that in pure Cu_2O. Furthermore, only an average coordination number of 1.2 can be assigned to this specimen, which makes the separation of a new Cu_2O phase under the influence of the pre-treatment unlikely. The presence of the Cu(I)-containing specimen in the s-$Cu_{0.4}Co_{2.6}$ sample can be demonstrated even more spectacularly by analyzing the truly informative XANES region. Indeed, a characteristic electronic transition in this energy range due to the 1 s-4p electric dipole, allows the oxidation states of copper to be distinguished. In particular, a well-established peak in the energy range 8980–8985 eV develops exclusively in Cu(I)-containing systems [55]. In this range of our pre-treated or spent samples, weak maxima were detected only for s-$Cu_{0.4}Co_{2.6}$ derivatives. Consequently, the presence of this poorly defined Cu(I)–O specimen can probably cause significant changes in the surface composition that led to the observed positive changes in the catalytic ability of the s-$Cu_{0.4}Co_{2.6}$ catalyst. However, the presence of this specimen can readily be attributed to the normal spinel structure, in which copper cations are stabilized to such an extent that their complete reduction can be excluded. These findings contradict apparently with the XRD results exhibiting the exclusive existence of metallic phases. It is noteworthy that the (powder) XRD method is severely limited in determining non-crystalline phases, while the XAS method is capable detecting the average coordination sphere of the metallic centers regardless of whether they occupy positions in crystalline or amorphous phases. The apparent contradiction can thus be resolved if the detected amorphous phases are considered as non-crystalline CoO.

Perhaps more surprisingly, complete reduction of the spinel structure by catalytic application in a reductive atmosphere and at an altered reaction temperature – leading to the formation of an alloy or bimetallic phases – only fully demonstrated for the s-$CuCo_2$ structure. In contrast, for two other spinel derivatives, the persistence of either CoO and/or Cu(I)–O specimens was found to define the differences in catalytic performance. Based on these findings, the high performance of s-$Cu_{0.4}Co_{2.6}$ can be associated with the appearance of the Cu(I)–O specimen which can probably cause significant changes in the surface composition that

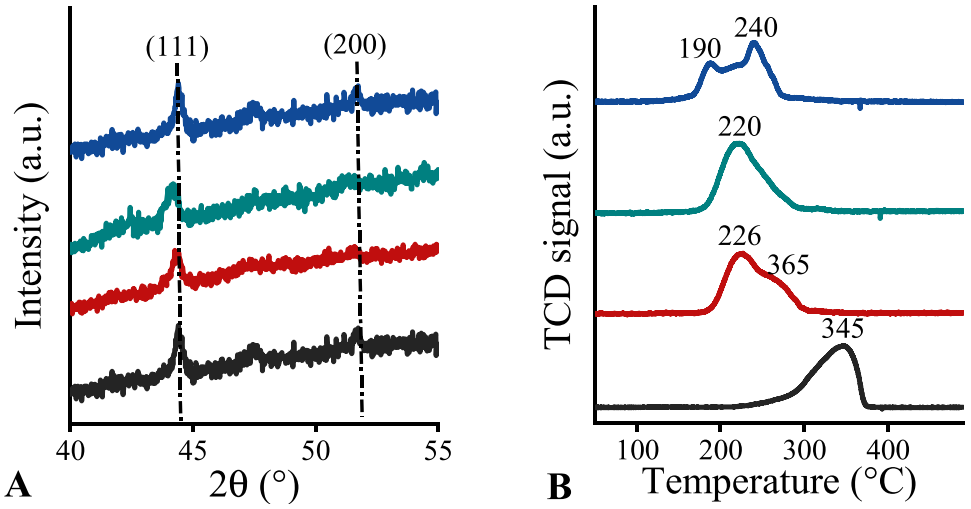

Fig. 5. XRD patterns (A) of the pre-treated and TPR curves (B) of the as-prepared s-Co_3 (black), s-$Cu_{0.1}Co_{2.9}$ (wine-colored), s-$Cu_{0.4}Co_{2.6}$ (cyan) and s-$CuCo_2$ (blue).

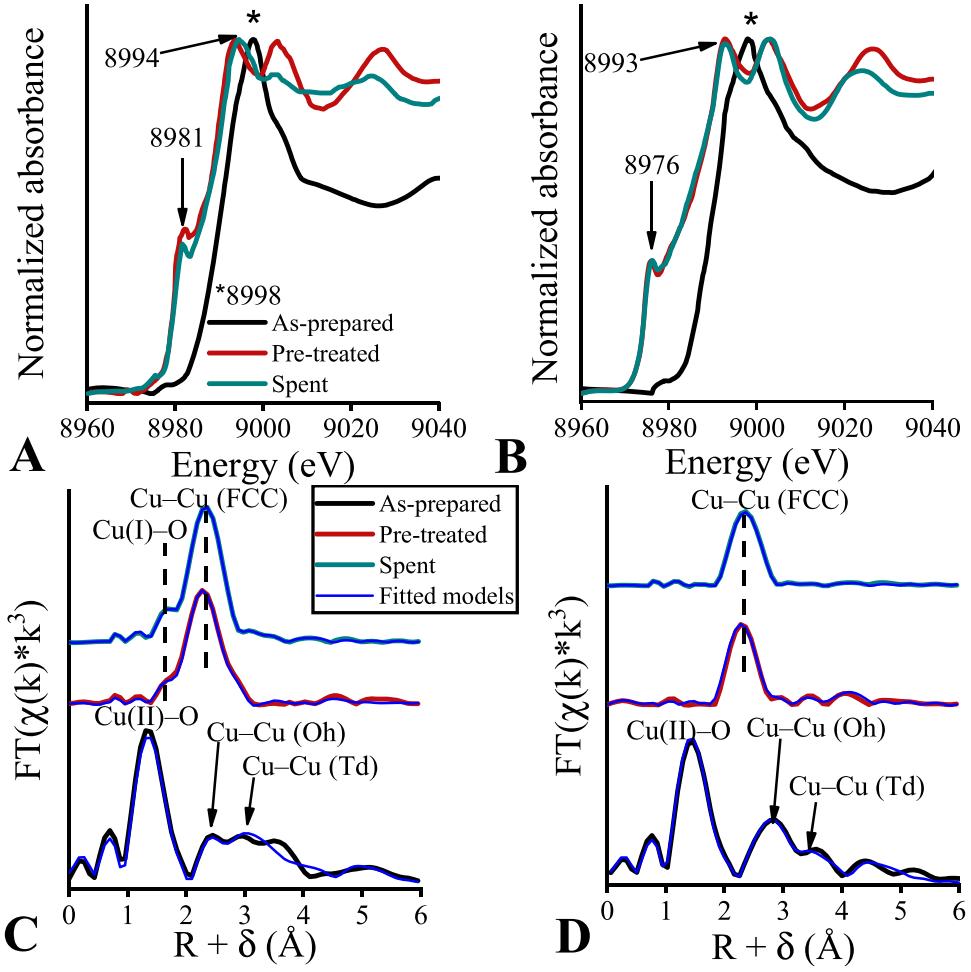

Fig. 6. XANES region of the Cu K-edge XAS spectra (A, B) and phase-corrected pseudo-radial distribution functions (C, D; generated by Fourier transformation (FT) of the corresponding EXAFS spectra) of the as-prepared (black) s-$Cu_{0.4}Co_{2.6}$ (A, C) and s-$CuCo_2$ (B, D) as well as their pre-treated (wine colored) and spent (cyan) counterparts.

led to the observed positive changes in catalytic ability.

To verify the above statement, *ex-situ* XPS studies were conducted on the spinels and their derivatives (Fig. 8). The XPS studies showed that Cu (II), Co(II) and Co(III) and the oxygen centers exclusively occupied the corresponding positions on the surfaces of the as-prepared structures (Fig. S6.) [56]. Compared to the initial state of the actual surfaces, where the copper centers are overrepresented as in the bulk, a significant redistribution of the active surfaces due to the pre-treatment was

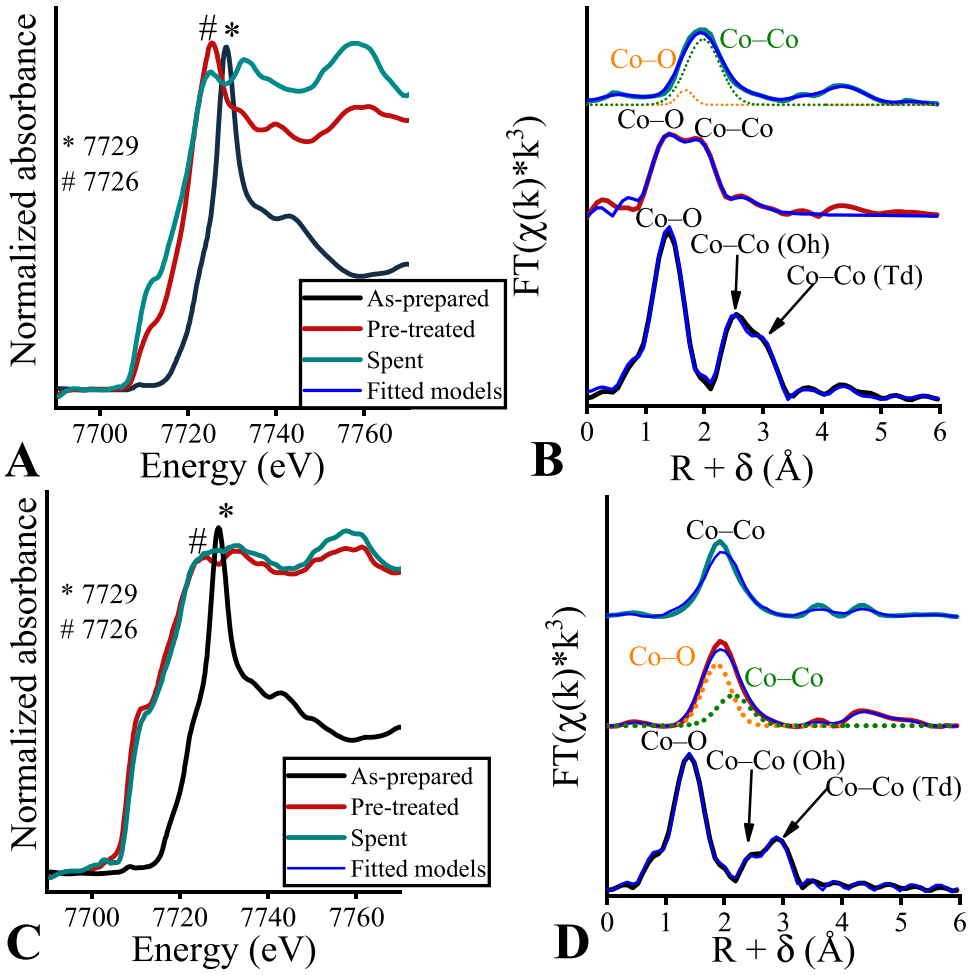

Fig. 7. XANES region of the Co K-edge XAS spectra (A, C) and phase-corrected pseudo-radial distribution functions (B, D; generated by Fourier transformation (FT) of the corresponding EXAFS spectra) of the as-prepared (black) s-$Cu_{0.4}Co_{2.6}$ (A, B) and s-$CuCo_2$ (C, D) as well as their pre-treated (wine-colored) and spent (cyan) counterparts.

observed, albeit in a significantly different manner from catalyst to catalyst. In each sample, the copper specimens were reduced completely during the pre-treatment and remained unchanged during the reaction [57]. When investigating the influence of pre-treatment on the surface composition, it was found that the Co 2p 3/2 peak of s-$Cu_{0.1}Co_{2.9}$ can be fitted via considering two components, in particular CoO [58] as well as (metallic) Co^0 specimens [59,60]. Moreover, the contribution of the parameters related to the oxide phases is remarkable (Table S5). The ratio between the metallic and oxidized cobalt phases is approximately Co^0: CoO = 55:45, but the ratio of copper-to-cobalt has not changed, so in this case there is an excess of cobalt. It is interesting to note that Co/CoO catalysts with almost the same molar ratio were found to be particularly inactive phase for CO_2 hydrogenation as reported [32,33]. The co-existence of this (CoO) oxide phase on the surface at this level may offer an explanation for the observed lower activity of this sample. As a result of the increase in the initial copper content (s-$Cu_{0.4}Co_{2.6}$), the active surface area was more reduced. Thus, the presence of the CoO and Co^0 specimens can only be realized on the surface of the corresponding sample. In addition, the metallic component dominates on the surface (Co^0: CoO = 70:30) more significantly, which is an advantage over the s-$Cu_{0.1}Co_{2.9}$ catalyst. Since the Cu(I)–O specimen cannot be identified by XPS combined with AES experiments at the surface, in contrast to the more bulk-sensitive EXAFS measurements, its direct influence on the catalytic performance can be excluded. Interestingly, no cobalt was detectable in the investigation of the s-$CuCo_2$ derivative sample due to copper migration, so that the entire surface was covered with elemental copper. It is known that metallic copper has only moderate activity in the catalytic RWGS reaction and produces almost exclusively carbon monoxide [31]. This is in good agreement with the catalytic results, which demonstrate both reduced activity and increased CO-selectivity of the $CuCo_2O_4$ catalyst compared to other copper-containing spinels. As far as copper migration is concerned, it can be assumed that the migration of metallic copper is inhibited to some extent in the presence of the bulk copper(I) oxide, which in the case of s-$Cu_{0.4}Co_{2.6}$ is probably due to the well-known disproportion equation. The disproportion could determine how many metallic copper centers appear on the surface at a given temperature. Therefore, in the presence of potential reaction partner (CO_2, H_2), the surface composition of s-$Cu_{0.4}Co_{2.6}$ must change depending on the reaction temperature. However, at a certain temperature, the structure could solidify, so its catalytic performance would have to remain unchanged over time. And this is exactly what we experienced in the robustness tests. Overall, this disproportion could lead to the formation of the most active Co/CoO_x/Cu surface/subsurface composition for CO_2 methanation.

After the reaction, each catalyst surface was completely reduced. While a slight enrichment of metallic copper can be seen for s-$Cu_{0.1}Co_{2.9}$ and s-$Cu_{0.4}Co_{2.6}$, a slight enrichment of cobalt took place for s-$CuCo_2$, likely creating a CuCo alloy on the surface. The ratios of different components determined by *ex-situ* XPS measurements are collected in Table S5. However, the experienced differences remained qualitatively. Consequently, under the influence of the reaction temperature, such a significant redistribution of the active surfaces occurred that completely

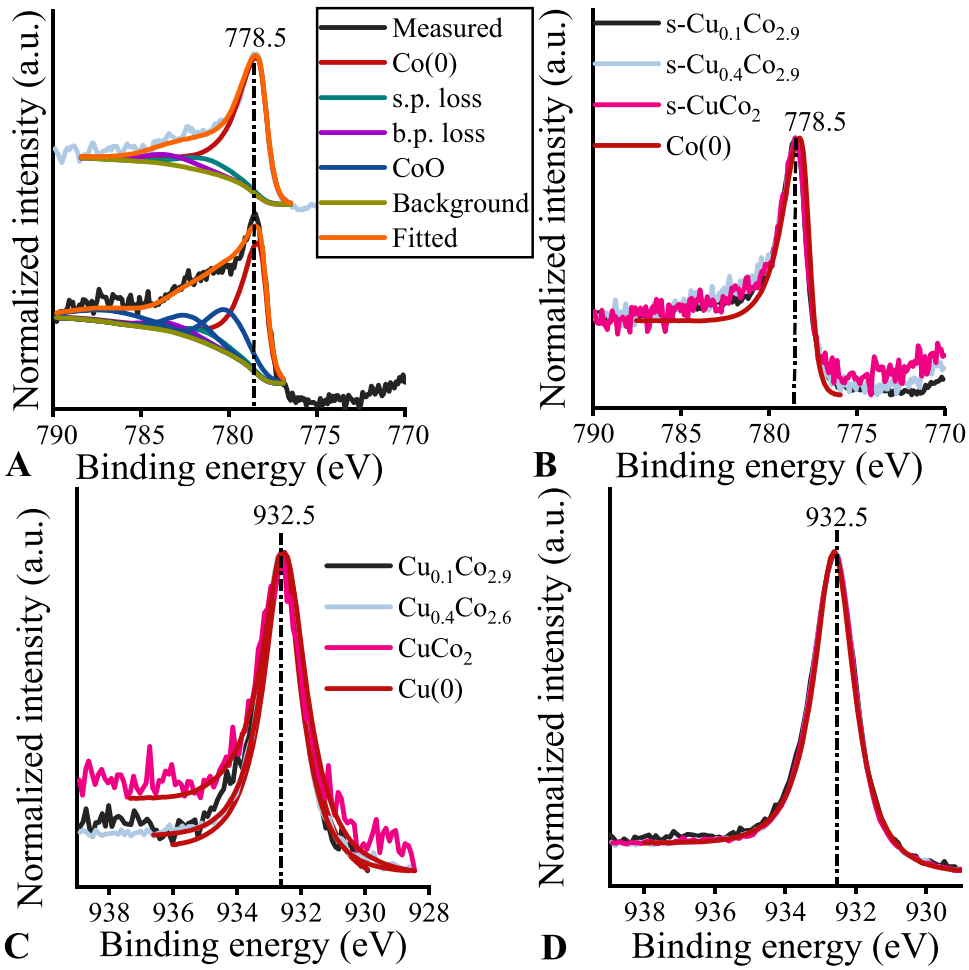

Fig. 8. *Ex-situ* Co 2p (A, B) and Cu 2p (C, D) XP spectra of the pre-treated (A, C) and spent (B, D) s-$Cu_{0.1}Co_{2.9}$ (black), s-$Cu_{0.4}Co_{2.6}$ (gray) and s-$CuCo_2$ (violet) structures.

new active surfaces emerged, which can be handled as completely different catalysts. This change can lead to the detected changes in the catalytic activity of the spinel derivatives at high temperatures.

To determine how the active surface area changes under the reaction conditions, NAP-XPS studies were carried out on the most efficient, s-$Cu_{0.4}Co_{2.6}$ catalyst (Fig. 9 (A, B)). It can be seen that the oxidation and reduction pre-treatment resulted in an almost completely metallic surface [57,59], as shown by the oxygen content of almost zero. Auger spectra of Cu L_3VV (Fig. 9 (C)) give additional information that Cu is also in metallic state. Furthermore, the surface layer was enriched with Cu compared to the initial bulk stoichiometry (Table S6).

Back to the results from NAP-XPS. The reaction at 300 °C did not lead to any significant changes in stoichiometry, apart from a slight relative increase in the Cu and O content in the surface layer. However, increasing the reaction temperature to 450 °C resulted in a further significant increase in the copper concentration to 50.8 at. percent, while the oxygen content remained low, indicating an almost metallic character of the surface region of the catalyst. All this shows that below 450 °C reaction temperature there are no significant changes in the active surfaces. In contrast, there may be a redistribution of the surface leading to the changes in catalytic performance. A more detailed interpretation of the NAP-XPS results can be seen in the Supporting information (Section S2.1.2).

To further confirm the fact of surface redistribution, TEM-EDS measurements were made (Figs. 10, S7 and S8). For this purpose, the surface ratio of the metallic specimens on the surface of s-$CuCo_2$ and s-$Cu_{0.4}Co_{2.6}$ catalysts was investigated. Due to the pre-treatment, the s-$Cu_{0.4}Co_{2.6}$ catalyst showed a "film-like" segregation of the copper samples, while the s-$CuCo_2$ catalyst showed well-distributed copper and cobalt centers. In this case, this does not contradict the results of the XPS studies, which showed the absence of the cobalt samples, as XPS is a more surface-sensitive technique. After the reaction, the situation reversed, suggesting that the dynamically changing active surfaces are likely the cause of the differences in catalytic performance. More likely, the migration of copper onto the surface of the s-$Cu_{0.4}Co_{2.6}$ catalyst occurred gradually throughout the catalytic process – perhaps leading to the formation of an alloy – while sintering of metallic copper likely occurred when the s-$CuCo_2$ catalyst was used. As a result, the actual ratio of copper and cobalt centers changed truly. Additionally, the sintered copper centers perform worse compared to the dispersed ones, as reported earlier [61]. This may mean that the differences that occur in s-$Cu_{0.4}Co_{2.6}$ and s-$CuCo_2$ methanation reactions, especially activities, at low temperature (300 °C) persist even after the temperature is increased. In addition, due to the sintered surface, large amounts of carbon residues are also seen (Fig. S8), which will be discussed in more detail in the next chapter. It is important to emphasize that these surfaces are pre-defined by the original structure of the spinels, which is closely related to their composition. It was, however, excluded that the changes in the compositions can importantly influence the basicity of the spinels since the CO_2-TPD profiles of the as-prepared structures were almost identical to each other (Fig. S9) [62].

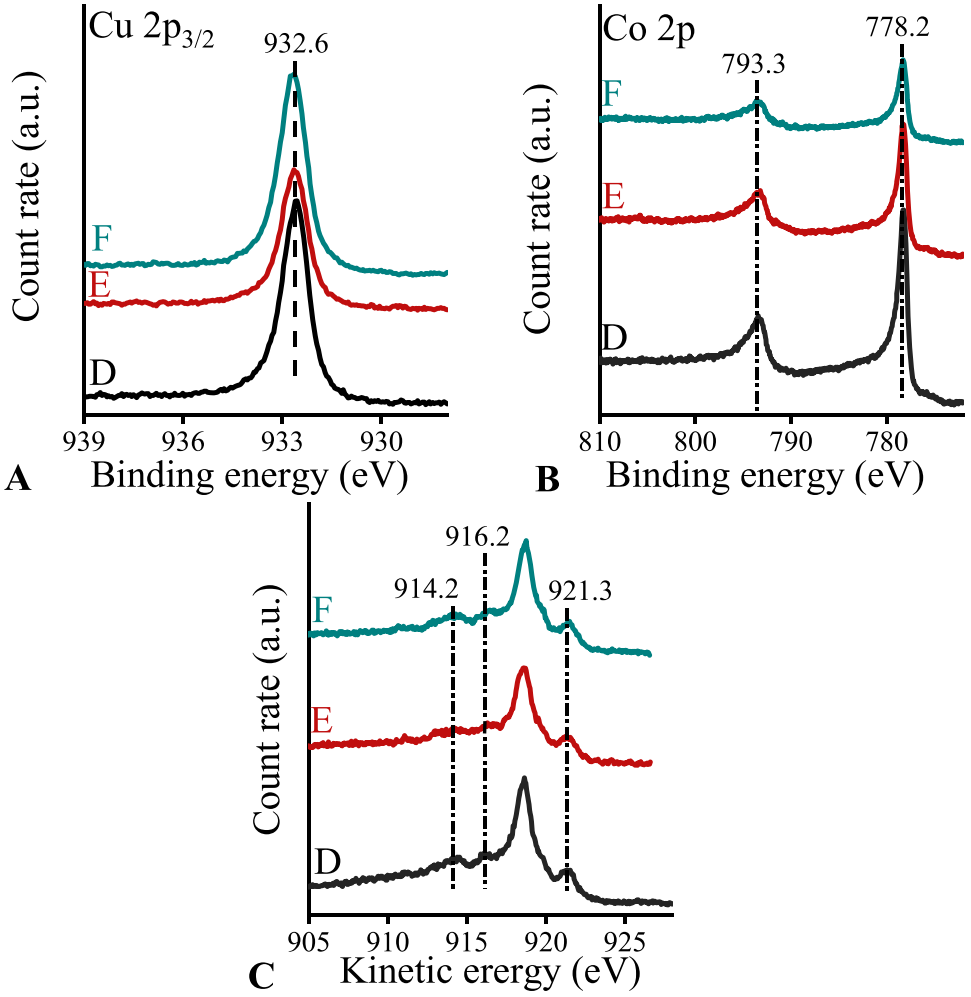

Fig. 9. Cu $2p_{3/2}$ (A) and Co 2p (B) NAP-XP spectra as well as Cu L_3VV (C) NAP-AE spectra of pre-treated (D), spent at 300 °C (E) and spent at 450 °C (F) s-$Cu_{0.4}Co_{2.6}$ structures.

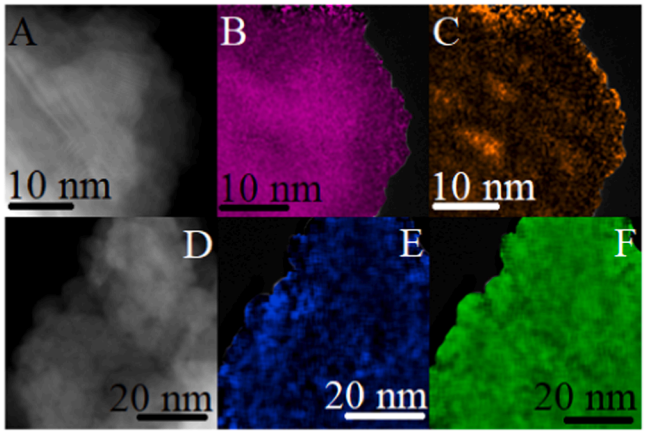

Fig. 10. HAADF TEM images (A, D), cobalt (B, E) and copper (C, F) distributions (detected by TEM-EDS) of pre-treated (A–C) and spent (D–F) s-$Cu_{0.4}Co_{2.6}$ structure.

3.4. Determination of the complex reaction network, mechanistic aspects

To identify the possible reaction intermediates and the composition of the gas phase in the CO_2 hydrogenation reaction, in-situ DRIFTS measurements were carried out under reaction conditions. It is generally accepted that the most important steps in CO_2 hydrogenation reactions are the dissociation of hydrogen and the vibrational or electronic activation of CO_2. Hydrogen dissociation is a simple step, especially when metallic particles are present. CO_2 activation depends strongly on the type of metal and oxide [63,64]. Therefore, we first focus on how CO_2 is adsorbed on the three different catalysts, CoOx, s-$Cu_{0.4}Co_{2.6}$ and s-$CuCo_2$. The DRIFT spectra after adsorption of CO_2 and subsequent heating in He are shown in Fig. S10. On the surface of pure CoOx, both the characteristic vibrational modes of anchored CO_2 and various types of carbonates and carboxylates [64,65] can be seen below 300 °C without He flashing. When the temperature was increased or He-flashing was used, the fingerprint region was dominated by the vibrational peaks of the monodentate carbonates. In contrast, when the surface of s-$CuCo_2$ is examined, the adsorption of monodentate carbonates [64] can be detected. Unfortunately, there is no clear evidence of CO_2 adsorption on the surface of s-$Cu_{0.4}Co_{2.6}$, only a weak, tiny vibrational band at 2050 cm^{-1} can be seen [64,65], which is associated with the adsorbed CO [29]. In separate experiments (not shown) the interaction of H_2 with adsorbed CO_2 was investigated. For these tests, the sample, after being exposed to CO_2 at room temperature, was heated in H_2. However, the newly formed sample under the influence of charged H_2 could not be determined.

By carrying out in-situ DRIFTS measurements under reaction conditions (Fig. 11), it can be realized that the mechanism of methanation differs depending on the catalyst used. Analysis of the gas phase exhibited the formation of methane (1305 and 3016 cm^{-1}) [29,66,67]

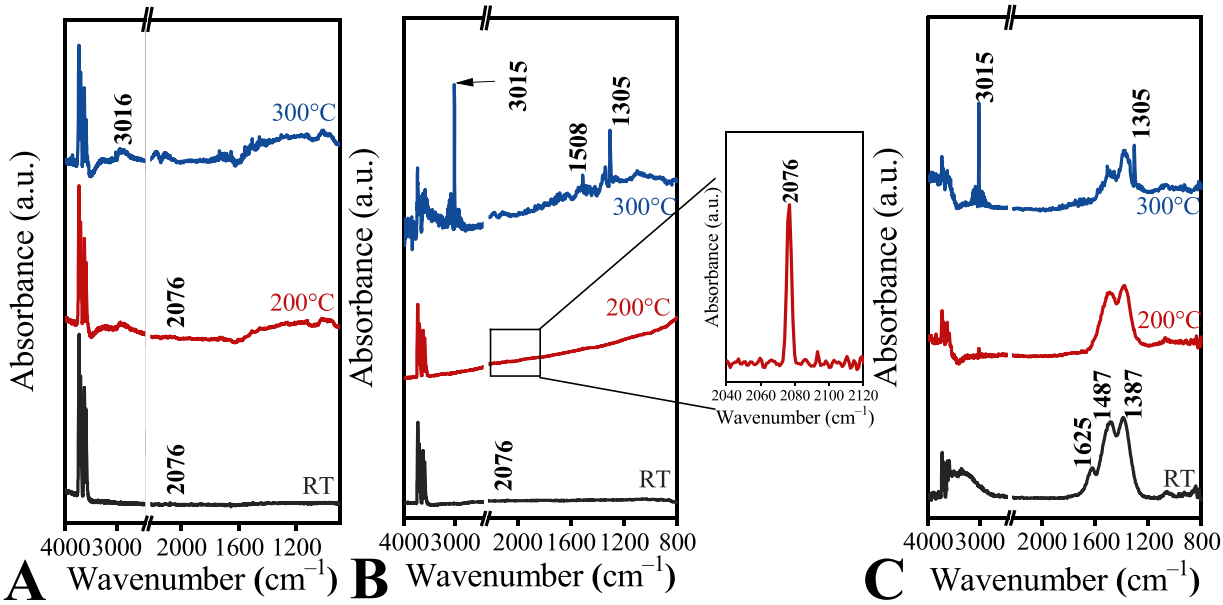

Fig. 11. *In-situ* DRIFT spectra of CoOx (A), s-$Cu_{0.4}Co_{2.6}$ (B) and s-$CuCo_2$ (C) spinel structure under reaction conditions of catalytic CO_2 methanation.

from 250 °C on each catalyst. It is essential to note that no formates of any kind were detected at either low or high temperatures. The spectra of s-$CuCo_2$ consisted of the linear combined characteristic vibration bands of carboxylates/bidentate carbonate (1625 cm^{-1}) and monodentate carbonates (1487 and 1387 cm^{-1}) [23,29,64,66,67] those existed at low temperature. Upon increasing the reaction temperature, the characteristic vibration bands of both carboxylates and carbonates start decrease in intensity. Based on these observations, a possible catalytic RWGS reaction promoted by spinel derivatives was detailed as follows.

Under the influence of hydrogen, the carboxylate (HOCO) can be converted into methane via the RWGS pathways [68]:

$$HOCO(a) \rightarrow CO(a) + OH(a) \quad (1)$$

$$CO(a) + H(a) \rightarrow HCO(a) \quad (2)$$

In the following steps, the HCO is further hydrogenated by forming H_2CO and then reacts readily to form methyl species with hydrogen:

$$HCO(a) + H(a) \rightarrow H_2CO(a) + 2H(a) \rightarrow H_3C(a) + OH(a) \quad (3)$$

$$H_3C(a) + H(a) \rightarrow CH_4(g) \quad (4)$$

It can be assumed that the carbonates in monodentate, bidentate or polydentate form are not involved in the reaction sequence. Moreover, these specimens may occupy certain active sites that may lead to surface poisoning and thus inhibition of the reaction. Furthermore, the adsorption of these carbonates probably leads to the formation of an amorphous carbon layer, which was seen on TEM-EDS when the surface is enriched with metallic cobalt due to the arrangement of the sintered copper. This reaction mechanism agrees well with the results of the structural analysis, which suggests a purely metallic surface as the active sample for the pre-treated s-$CuCo_2$ sample. In fact, metallic copper was previously identified as an active, but CO selective catalyst for the RWGS reaction.

Surprisingly, no intermediates are detectable in the analysis of s-$Cu_{0.4}Co_{2.6}$ and CoOx samples (Fig. 11 (A, B)). Only the determination of a small amount of CO succeeded exclusively at 200 °C or below. In the absence of intermediates, it is difficult to say how the reaction took place. However, it is likely that CO played the key role in the methanations. The main fraction of CO cannot be further hydrogenated, but its dissociation can occur very rapidly at an active surface, producing surface or subsurface carbon specimens. Since the dissociation of CO on the cobalt surface in the Fischer-Tropsch reaction has already been proposed [69], the formation of highly active carbon during the interaction of the reaction mixture with the catalyst surface at an early stage of the reaction is very likely. In order to justify the key role of active carbon, isothermal experiments were performed at 225 °C.

The fingerprint-like vibrational bands of methane (3016 cm^{-1}) and CO (2076 cm^{-1}) were observed as a function of time (Fig. 12). When the CO_2 flow is closed, the CO band disappears and the CH_4 peak remains. This clearly shows that activated carbon can be converted to methane on the cobalt or cobalt/copper surfaces. Furthermore, both peaks recover as expected in a $CO_2 + H_2$ mixture. In the absence of H_2 loading, only the CO band remains. Thus, the actual catalyst is not able to shop activated (dissociated) hydrogen on its surface.

It follows that the methanations promoted by s-$Cu_{0.4}Co_{2.6}$ and CoOx samples build up a three-step reaction cascade. In the first step, hydrogen-assisted CO_2 dissociation likely occurs through the formation of thermodynamically unstable carboxylates and/or bicarbonates that decompose at the Co/CoOx interface (Eqs. (1) and (2)). In the second step, C–O bond cleavage, adsorbed CO (Eq. (5)) or formyl-like (HCO) samples are probably involved. This may lead to the formation of active surface/subsurface carbon. Since a low intensity CO was found in a narrow temperature range instead of formyl, it is possible that not as much hydrogen is required for C–O bond cleavage as was assumed when using cobalt-based Fischer-Tropsch catalysts [69].

$$CO(a) \rightarrow C(a) + O(a) \quad (5)$$

$$C(a) + 4H(a) \rightarrow CH_4 \quad (6)$$

In the last step (Eq. (6)), the hydrogenation of the active carbon probably takes place. The conversion of the active carbon into methane by alkyl fragments must be an extremely fast process, because no hydrocarbon fragments can be seen in the spectra of DRIFT. This rapid hydrogenation probably takes place at a highly active $Cox(CoO)_{1-x}$ site, as has been reported recently [32]. In this scenario, the metallic cobalt sample is able to act as an electronic catalytic site providing electrons for the hydrogenation steps. A more detailed interpretation of the DRIFTS results can be seen in the Supporting information (Section S2.2).

The proposed mechanism (depicted in Scheme 1) is also supported by the characterization results. In the case of s-$Cu_{0.4}Co_{2.6}$, a well-formed $Cu^0/Co^0/CoO$ surface is formed due to the pre-treatment (XPS, EXAFS). In its formation, the presence of the subsurface Cu(I)–O specimen likely

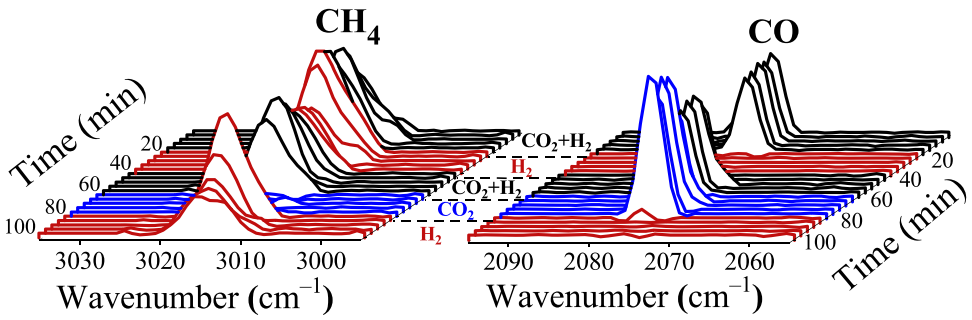

Fig. 12. Isothermal catalytic CO_2 hydrogenation reactions as a function of time altering gas mixture at 225 °C, over activated s-$Cu_{0.4}Co_{2.6}$ catalyst.

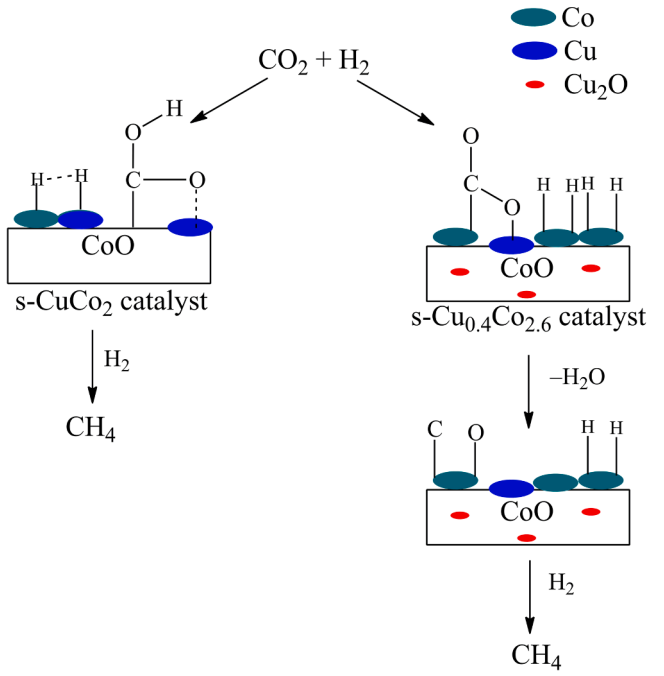

Scheme 1. Proposed reaction mechanisms of CO_2 methanation catalyzed by different activated spinel structures (s-$CuCo_2$ and s-$Cu_{0.4}Co_{2.6}$).

acts an important role, as it prevents the complete reduction of the copper content and thus the enrichment of metallic copper on the surface. It is easy to see that the active sites (Co/CoO) for efficient methanation are present. When these active sites are no longer accessible at higher temperatures (> 450 °C) due to surface redistribution, the efficiency of hydrogenation decreases, which may explain the unanticipated decrease in activity of this sample at 550 °C. In this system, the main contribution of the Cu^0 centers comes rather from those that can ensure the formation of the appropriate mixture of metallic and oxidized cobalt on the surface. However, for this purpose, the ideal copper content must be found, otherwise more inactive (s-$Cu_{0.1}Co_{2.9}$ → Co_3O_4/CoO/Co/Cu surface) or completely different (s-$CuCo_2$ → Cu^0 surface) surfaces will form. Moreover, the Cu^0 centers are also able to promote the first step of the mechanism. This is the main reason why this catalyst has been shown to be about 4 times more active than Co/CoOx catalysts reported previously [32].

4. Conclusions

It was hypothesized that highly efficient Cu-Co bimetallic catalysts for thermo-catalytic CO_2 methanation are generated from spinel oxide precursors and their surface composition and catalytic performance are fine-tuned by changing the cation ratio of the spinel precursors. Spinel structures with different copper-cobalt ratios were prepared and investigated in a CO_2 hydrogenation reaction following an oxidative-reductive two-step activation procedure. Each spinel derivative was able to promote the reaction, but there were significant differences in both their activity and selectivity. The $Cu_{0.4}Co_{2.6}O_4$ derivative proved to be the most efficient, robust and regenerable catalyst for the selective production of methane, even in a relatively high temperature range between 250 and 425 °C. This high performance was closely related to the surface composition of the actual (pre-treated) catalyst. It became clear that neither the highly oxidized surface with cobalt excess ($Cu_{0.1}Co_{2.9}O_4$) consisting of CoO/Co^0 + Cu^0 nor the highly reduced surface with pure metallic copper ($CuCo_2O_4$) are able to efficiently promote methanation due to copper migration. For best performance, the formation of Co/CoO centers on a surface enriched with metallic copper is required. However, the reducibility of the catalytic surfaces depends on the composition of the spinel precursor and most likely on their structure. The most efficient $Cu_{0.4}Co_{2.6}O_4$ possessed an almost normal spinel structure in which the Cu(II) centers were almost exclusively in tetrahedral coordinated crystal positions. This may affect the redox equilibrium and prevent the complete reduction of copper content leading to the formation of subsurface Cu(I)-containing specimens and the most active surface composition. In contrast, the other two structures had mixed spinel structures where the complete reduction of the copper content occurred in the absence of overstabilization, that was attached to a normal spinel structure. The investigation of the reaction mechanism also showed that the mechanistic aspects also changed depending on the copper content and thus on the surface composition. While catalysts with lower copper content probably provide the methane via a three-step cascade reaction consisting of 1, hydrogen-assisted CO_2 dissociation, 2, C–O bond cleavage of the adsorbed CO and 3, hydrogenation of the active carbon at the surface, a "simple" RWGS reaction was proposed for catalysts with a copper to cobalt ratio of 1:2. This shows that the active carbon at the surface or subsurface plays a key role in the mechanism when a lower copper content is used. This phenomenon is the same as that reported for catalysts with Co/CoO_X active centers in Fischer-Tropsch reactions. Based on this analogy, we can assume that despite the metallic ratio in the $Cu_{0.4}Co_{2.6}O_4$ catalyst, the Co/CoO_X centers have the most important catalytic function, but the metallic copper/oxide centers dominate their formation and also act as co-catalysts in the reaction.

CRediT authorship contribution statement

Gábor Varga: Conceptualization, Methodology, Formal analysis, Investigation (structural, EXAFS), Writing – original draft, Writing – review & editing, Visualization, Supervision. **Imre Szenti:** Methodology, Formal analysis, Investigation (catalytic reactions, DRIFTS), Validation, Formal analysis, Visualization. **János Kiss:** Formal analysis, Conceptualization, Investigation (DRIFTS), Writing – original draft. **Kornélia Baán:** Formal analysis, Investigation (DRIFTS, TPD, BET). **Gyula Halasi:** Formal analysis, Investigation (catalytic reactions, NAP-XPS). **László Óvári:** Formal analysis, Investigation (NAP-XPS). **Ákos**

Szamosvölgyi: Formal analysis, Investigation (XPS). **Róbert Mucsi:** Formal analysis, Investigation (catalytic reactions). **Erzsébet Dodony:** Formal analysis, Investigation (TEM, TEM-EDX). **Zsolt Fogarassy:** Formal analysis, Investigation (TEM, TEM-EDX). **Béla Pécz:** Formal analysis, Investigation (TEM, TEM-EDX). **Luca Olivi:** Investigation (EXAFS). **András Sápi:** Conceptualization, Methodology, Writing – original draft, Writing – review & editing, Visualization, Supervision, Funding acquisition. **Ákos Kukovecz:** Data curation, Resources, Funding acquisition. **Zoltán Kónya:** Data curation, Resources, Funding acquisition.

Author contributions

The manuscript was written through contributions of all authors. All authors have given approval to the final version of the manuscript.

Declaration of Competing Interest

The authors declare that they have no known competing financial interests or personal relationships that could have appeared to influence the work reported in this paper.

Data availability

Data will be made available on request.

Acknowledgments

As gratefully acknowledges the support of the Bolyai Janos Research Fellowship of the Hungarian Academy of Science and the "UNKP-21-5-SZTE-586" New National Excellence Program as well as the funding provided by the Indo-Hungarian TÉT Project (2019-2.1.13-TÉT_IN-2020-00015) of the Ministry for Innovation and Technology from the source of the National Research, Development and Innovation Fund. The Ministry of Human Capacities through the EFOP-3.6.1-16-2016-00014 project and the 20391-3/2018/FEKUSTRAT are acknowledged. The authors acknowledge the supports of Hungarian OTKA projects Nos. 138714 and SNN_135918 project for the Hungarian National Research, Development and Innovation Office. Project no. TKP2021-NVA-19 has been implemented with the support provided by the Ministry of Innovation and Technology of Hungary from the National Research, Development and Innovation Fund, financed under the TKP2021-NVA funding scheme. Project no. RRF-2.3.1-21-2022-00009, titled National Laboratory for Renewable Energy has been implemented with the support provided by the Recovery and Resilience Facility of the European Union within the framework of Programme Széchenyi Plan Plus. The ELI-ALPS project (GINOP-2.3.6-15-2015-00001) is supported by the European Union and co-financed by the European Regional Development Fund. The XAFS beamline of Elettra is greatly acknowledged for allowing the XAS measurements.This work was also supported by the University of Szeged Open Access Fund (Grant number: 6524).

Appendix A. Supporting information

Supplementary data associated with this article can be found in the online version at doi:10.1016/j.jcou.2023.102582.

References

[1] K. Loza, M. Heggen, M. Epple, Synthesis, structure, properties, and applications of bimetallic nanoparticles of noble metals, Adv. Funct. Mater. 30 (2020) 1909260, https://doi.org/10.1002/adfm.201909260.

[2] Y. Zou, X. Wang, A. Khan, P. Wang, Y. Liu, A. Alsaedi, T. Hayat, X. Wang, Environmental remediation and application of nanoscale zero-valent iron and its composites for the removal of heavy metal ions: a review, Environ. Sci. Technol. 50 (2016) 7290–7304, https://doi.org/10.1021/acs.est.6b01897.

[3] P. Babakhani, T. Phenrat, M. Baalousha, K. Soratana, C.L. Peacock, B.S. Twining, M.F. Hochella, Potential use of engineered nanoparticles in ocean fertilization for large-scale atmospheric carbon dioxide removal, Nat. Nanotechnol. 17 (2022) 1342–1351, https://doi.org/10.1038/s41565-022-01226-w.

[4] O. Antonoglou, J. Moustaka, I.D.S. Adamakis, I. Sperdouli, A.A. Pantazaki, M. Moustakas, C. Dendrinou-Samara, Nanobrass CuZn nanoparticles as foliar spray nonphytotoxic fungicides, ACS Appl. Mater. Interfaces 10 (2018) 4450–4461, https://doi.org/10.1021/acsami.7b17017.

[5] J.A. Gutiérrez, S. Caballero, L.A. Díaz, M.A. Guerrero, J. Ruiz, C.C. Ortiz, High antifungal activity against candida species of monometallic and bimetallic nanoparticles synthesized in nanoreactors, ACS Biomater. Sci. Eng. 4 (2018) 647–653, https://doi.org/10.1021/acsbiomaterials.7b00511.

[6] P. Zeng, C. Liu, X. Zhao, C. Yuan, Y. Chen, H. Lin, L. Zhang, Enhanced catalytic conversion of polysulfides using bimetallic Co_7Fe_3 for high-performance lithium-sulfur batteries, ACS Nano 14 (2020) 11558–11569, https://doi.org/10.1021/acsnano.0c04054.

[7] P. Wu, Z. He, Y. Liu, L. Song, C. Wang, E. Muhumuza, P. Bai, L. Zhao, S. Mintova, Z. Yan, Compatibility between activity and selectivity in catalytic oxidation of benzyl alcohol with Au-Pd nanoparticles through redox switching of SnOx, ACS Appl. Mater. Interfaces 13 (2021) 49780–49792, https://doi.org/10.1021/acsami.1c10207.

[8] C. Liu, C. Ji, T. Zhou, X. Hong, M. Szostak, Bimetallic cooperative catalysis for decarbonylative heteroarylation of carboxylic acids via C-O/C-H coupling, Angew. Chem. 133 (2021) 10785–10794, https://doi.org/10.1002/ange.202100949.

[9] J.A. Schwarz, C.T. Ugbor, R. Zhang, The adsorption/impregnation of Pd(II) cations on alumina, silica, and their composite oxides, J. Catal. 138 (1992) 38–54, https://doi.org/10.1016/0021-9517(92)90005-3.

[10] J. Zhang, C.D. Sewell, H. Huang, Z. Lin, Closing the anthropogenic chemical carbon cycle toward a sustainable future via CO_2 valorization, Adv. Energy Mater. 11 (2021) 1–38, https://doi.org/10.1002/aenm.202102767.

[11] A. Parastaev, V. Muravev, E. Huertas Osta, A.J.F. van Hoof, T.F. Kimpel, N. Kosinov, E.J.M. Hensen, Boosting CO_2 hydrogenation via size-dependent metal–support interactions in cobalt/ceria-based catalysts, Nat. Catal. 3 (2020) 526–533, https://doi.org/10.1038/s41929-020-0459-4.

[12] R.G. dos Santos, A.C. Alencar, Biomass-derived syngas production via gasification process and its catalytic conversion into fuels by Fischer Tropsch synthesis: a review, Int. J. Hydrog. Energy 45 (2020) 18114–18132, https://doi.org/10.1016/j.ijhydene.2019.07.133.

[13] K. Teramura, T. Tanaka, S. Kikkawa, H. Asakura, S. Hosokawa, Ni−Pt alloy nanoparticles with isolated Pt atoms and their cooperative neighboring Ni atoms for selective hydrogenation of CO_2 toward CH_4 evolution: in situ and transient Fourier transform infrared studies, ACS Appl. Nano Mater. 3 (2020) 9633–9644, https://doi.org/10.1021/acsanm.0c01570.

[14] B. Mutz, M. Belimov, W. Wang, P. Sprenger, M.A. Serrer, D. Wang, P. Pfeifer, W. Kleist, J.D. Grunwaldt, Potential of an alumina-supported Ni_3Fe catalyst in the methanation of CO_2: impact of alloy formation on activity and stability, ACS Catal. 7 (2017) 6802–6814, https://doi.org/10.1021/acscatal.7b01896.

[15] E. Le Saché, L. Pastor-Pérez, B.J. Haycock, J.J. Villora-Picó, A. Sepúlveda-Escribano, T.R. Reina, Switchable catalysts for chemical CO_2 recycling: a step forward in the methanation and reverse water-gas shift reactions, ACS Sustain. Chem. Eng. 8 (2020) 4614–4622, https://doi.org/10.1021/acssuschemeng.0c00551.

[16] H. Arandiyan, Y. Wang, J. Scott, S. Mesgari, H. Dai, R. Amal, In situ exsolution of bimetallic Rh-Ni nanoalloys: a highly efficient catalyst for CO_2 methanation, ACS Appl. Mater. Interfaces 10 (2018) 16352–16357, https://doi.org/10.1021/acsami.8b00889.

[17] L. Xu, Y. Cui, M. Chen, X. Wen, C. Lv, X. Wu, C.E. Wu, Z. Miao, X. Hu, Screening transition metals (Mn, Fe, Co, and Cu) promoted Ni-based CO_2 methanation bimetal catalysts with advanced low-temperature activities, Ind. Eng. Chem. Res. 60 (2021) 8056–8072, https://doi.org/10.1021/acs.iecr.1c00656.

[18] G.L. Bezemer, J.H. Bitter, H.P.C.E. Kuipers, H. Oosterbeek, J.E. Holewijn, X. Xu, F. Kapteijn, A.J. Van Diilen, K.P. De Jong, Cobalt particle size effects in the Fischer-Tropsch reaction studied with carbon nanofiber supported catalysts, J. Am. Chem. Soc. 128 (2006) 3956–3964, https://doi.org/10.1021/ja058282w.

[19] I.K. Van Ravenhorst, A.S. Hoffman, C. Vogt, A. Boubnov, N. Patra, R. Oord, C. Akatay, F. Meirer, S.R. Bare, B.M. Weckhuysen, On the cobalt carbide formation in a Co/TiO_2 Fischer-Tropsch synthesis catalyst as studied by high-pressure, long-term operando X-ray absorption and diffraction, ACS Catal. 11 (2021) 2956–2967, https://doi.org/10.1021/acscatal.0c04695.

[20] A. Karelovic, P. Ruiz, CO_2 hydrogenation at low temperature over Rh/γ-Al_2O_3 catalysts: effect of the metal particle size on catalytic performances and reaction mechanism, Appl. Catal. B Environ. 113–114 (2012) 237–249, https://doi.org/10.1016/j.apcatb.2011.11.043.

[21] M. Duan, L. Jiang, G. Zeng, D. Wang, W. Tang, J. Liang, H. Wang, D. He, Z. Liu, L. Tang, Bimetallic nanoparticles/metal-organic frameworks: synthesis, applications and challenges, Appl. Mater. Today 19 (2020) 100564, https://doi.org/10.1016/j.apmt.2020.100564.

[22] Sonal, K.K. Pant, S. Upadhyayula, An insight into the promotional effect on Fe-Co bimetallic catalyst in the Fischer Tropsch reaction: a DRIFTS study, Fuel 276 (2020), 118044, https://doi.org/10.1016/j.fuel.2020.118044.

[23] G. Varga, A. Sápi, T. Varga, K. Baán, I. Szenti, G. Halasi, R. Mucsi, L. Óvári, J. Kiss, Z. Fogarassy, B. Pécz, Á. Kukovecz, Z. Kónya, Ambient pressure CO_2 hydrogenation over a cobalt/manganese-oxide nanostructured interface: a combined in situ and ex situ study, J. Catal. 386 (2020) 70–80, https://doi.org/10.1016/j.jcat.2020.03.028.

[24] D.V. Cesar, C.A. Peréz, V.M.M. Salim, M. Schmal, Stability and selectivity of bimetallic Cu-Co/SiO_2 catalysts for cyclohexanol dehydrogenation, Appl. Catal. A Gen. 176 (1999) 205–212, https://doi.org/10.1016/S0926-860X(98)00245-2.

[25] F. Conrad, C. Massue, S. Kühl, E. Kunkes, F. Girgsdies, I. Kasatkin, B. Zhang, M. Friedrich, Y. Luo, M. Armbrüster, G.R. Patzke, M. Behrens, Microwave-hydrothermal synthesis and characterization of nanostructured copper substituted ZnM_2O_4 (M = Al, Ga) spinels as precursors for thermally stable Cu catalysts, Nanoscale 4 (2012) 2018–2028, https://doi.org/10.1039/c2nr11804a.

[26] L. Wang, L. Wang, J. Zhang, X. Liu, H. Wang, W. Zhang, Q. Yang, J. Ma, X. Dong, S. J. Yoo, J.G. Kim, X. Meng, F.S. Xiao, Selective hydrogenation of CO_2 to ethanol over cobalt catalysts, Angew. Chem. Int. Ed. 57 (2018) 6104–6108, https://doi.org/10.1002/anie.201800729.

[27] J. Graciani, K. Mudiyanselage, F. Xu, A.E. Baber, J. Evans, S.D. Senanayake, D. J. Stacchiola, P. Liu, J. Hrbek, J.F. Sanz, J.A. Rodriguez, Highly active copper-ceria and copper-ceria-titania catalysts for methanol synthesis from CO_2, Science 345 (2014) 546–550, https://doi.org/10.1126/science.1253057.

[28] T. Fan, H. Liu, S. Shao, Y. Gong, G. Li, Z. Tang, Cobalt catalysts enable selective hydrogenation of CO_2 toward diverse products: recent progress and perspective, J. Phys. Chem. Lett. 12 (2021) 10486–10496, https://doi.org/10.1021/acs.jpclett.1c03043.

[29] A. Efremova, T. Rajkumar, Á. Szamosvölgyi, A. Sápi, K. Baán, I. Szenti, J. Gómez-Pérez, G. Varga, J. Kiss, G. Halasi, Á. Kukovecz, Z. Kónya, Complexity of a Co_3O_4 system under ambient-pressure CO_2 methanation: influence of bulk and surface properties on the catalytic performance, J. Phys. Chem. C 125 (2021) 7130–7141, https://doi.org/10.1021/acs.jpcc.0c09717.

[30] J. Xie, P.P. Paalanen, T.W. van Deelen, B.M. Weckhuysen, M.J. Louwerse, K.P. de Jong, Promoted cobalt metal catalysts suitable for the production of lower olefins from natural gas, Nat. Commun. 10 (2019) 1–10, https://doi.org/10.1038/s41467-018-08019-7.

[31] M. Bersani, K. Gupta, A.K. Mishra, R. Lanza, S.F.R. Taylor, H.U. Islam, N. Hollingsworth, C. Hardacre, N.H. De Leeuw, J.A. Darr, Combined EXAFS, XRD, DRIFTS, and DFT study of nano copper-based catalysts for CO_2 hydrogenation, ACS Catal. 6 (2016) 5823–5833, https://doi.org/10.1021/acscatal.6b01529.

[32] K. Zhao, M. Calizzi, E. Moioli, M. Li, A. Borsay, L. Lombardo, R. Mutschler, W. Luo, A. Züttel, Unraveling and optimizing the metal-metal oxide synergistic effect in a highly active $Co_x(CoO)_{1-x}$ catalyst for CO_2 hydrogenation, J. Energy Chem. 53 (2020) 241–250, https://doi.org/10.1016/j.jechem.2020.05.025.

[33] I.C.T. Have, J.J.G. Kromwijk, M. Monai, D. Ferri, E.B. Sterk, F. Meirer, B. M. Weckhuysen, Uncovering the reaction mechanism behind CoO as active phase for CO_2 hydrogenation, Nat. Commun. 13 (2022) 324, https://doi.org/10.1038/s41467-022-27981-x.

[34] J. Su, Z. Zhang, D. Fu, D. Liu, X.C. Xu, B. Shi, X. Wang, R. Si, Z. Jiang, J. Xu, Y. F. Han, Higher alcohols synthesis from syngas over $CoCu/SiO_2$ catalysts: dynamic structure and the role of Cu, J. Catal. 336 (2016) 94–106, https://doi.org/10.1016/j.jcat.2016.01.015.

[35] Y. Xiang, V. Chitry, P. Liddicoat, P. Felfer, J. Cairney, S. Ringer, N. Kruse, Long-chain terminal alcohols through catalytic CO hydrogenation, J. Am. Chem. Soc. 135 (2013) 7114–7117, https://doi.org/10.1021/ja402512r.

[36] G. Zhang, G. Fan, L. Zheng, F. Li, Ga-promoted CuCo-based catalysts for efficient CO_2 hydrogenation to ethanol: the key synergistic role of Cu-CoGaOx interfacial sites, ACS Appl. Mater. Interfaces 14 (2022) 35569–35580, https://doi.org/10.1021/acsami.2c07252.

[37] H.T. Luk, C. Mondelli, D.C. Ferré, J.A. Stewart, J. Pérez-Ramírez, Status and prospects in higher alcohols synthesis from syngas, Chem. Soc. Rev. 46 (2017) 1358–1426, https://doi.org/10.1039/c6cs00324a.

[38] Y. Xiang, N. Kruse, Cobalt–copper based catalysts for higher terminal alcohols synthesis via Fischer–Tropsch reaction, J. Energy Chem. 25 (2016) 895–906, https://doi.org/10.1016/j.jechem.2016.09.014.

[39] S. Liu, C. Yang, S. Zha, D. Sharapa, F. Studt, Z. Zhao, J. Gong, Moderate surface segregation promotes selective ethanol production in CO_2 hydrogenation reaction over CoCu catalysts, Angew. Chem. 134 (2022), e202109027, https://doi.org/10.1002/ange.202109027.

[40] C. Huang, P. Ma, R. Wang, W. Li, J. Wang, H. Li, Y. Tan, L. Luo, X. Li, J. Bao, CuCo alloy nanonets derived from $CuCo_2O_4$ spinel oxides for higher alcohols synthesis from syngas, Catal. Sci. Technol. 11 (2021) 7617–7623, https://doi.org/10.1039/d1cy01179k.

[41] D. Klissurski, E. Uzunova, K. Ivanov, Binary spinel cobaltites of nickel, copper and zinc as precursors of catalysts for carbon oxides methanation, Catal. Lett. 15 (1992) 385–391, https://doi.org/10.1007/BF00769162.

[42] R. Nafria, A. Genç, M. Ibáñez, J. Arbiol, P. Ramírez De La Piscina, N. Homs, A. Cabot, Co-Cu nanoparticles: synthesis by galvanic replacement and phase rearrangement during catalytic activation, Langmuir 32 (2016) 2267–2276, https://doi.org/10.1021/acs.langmuir.5b04622.

[43] A. Remiro, A. Arandia, L. Oar-Arteta, J. Bilbao, A.G. Gayubo, Regeneration of $NiAl_2O_4$ spinel type catalysts used in the reforming of raw bio-oil, Appl. Catal. B Environ. 237 (2018) 353–365, https://doi.org/10.1016/j.apcatb.2018.06.005.

[44] N. Fairley, V. Fernandez, M. Richard-Plouet, C. Guillot-Deudon, J. Walton, E. Smith, D. Flahaut, M. Greiner, M. Biesinger, S. Tougaard, D. Morgan, J. Baltrusaitis, Systematic and collaborative approach to problem solving using X-ray photoelectron spectroscopy, Appl. Surf. Sci. Adv. 5 (2021), 100112, https://doi.org/10.1016/j.apsadv.2021.100112.

[45] X. Xiao, Z. Zhang, L. Cai, Y. Li, Z. Yan, Y. Wang, The excellent catalytic activity for thermal decomposition of ammonium perchlorate using porous $CuCo_2O_4$ synthesized by template-free solution combustion method, J. Alloy. Compd. 797 (2019) 548–557, https://doi.org/10.1016/j.jallcom.2019.05.074.

[46] L.H. Ai, J. Jiang, Rapid synthesis of nanocrystalline Co_3O_4 by a microwave-assisted combustion method, Powder Technol. 195 (2009) 11–14, https://doi.org/10.1016/j.powtec.2009.05.006.

[47] X.C. Dong, H. Xu, X.W. Wang, Y.X. Huang, M.B. Chan-Park, H. Zhang, L.H. Wang, W. Huang, P. Chen, 3D graphene-cobalt oxide electrode for high-performance supercapacitor and enzymeless glucose detection, ACS Nano 6 (2012) 3206–3213, https://doi.org/10.1021/nn300097q.

[48] J. Jacob, M.A. Khadar, Investigation of mixed spinel structure of nanostructured nickel ferrite, J. Appl. Phys. 107 (2010) 114310, https://doi.org/10.1063/1.3429202.

[49] H.Y. Chen, J.H. Chen, Preparation of p-type $CuCo_2O_4$ thin films by sol-gel processing, Mater. Lett. 188 (2017) 63–65, https://doi.org/10.1016/j.matlet.2016.10.096.

[50] J. Wang, P.A. Chernavskii, A.Y. Khodakov, Y. Wang, Structure and catalytic performance of alumina-supported copper-cobalt catalysts for carbon monoxide hydrogenation, J. Catal. 286 (2012) 51–61, https://doi.org/10.1016/j.jcat.2011.10.012.

[51] G. Jacobs, J.A. Chaney, P.M. Patterson, T.K. Das, B.H. Davis, Fischer-Tropsch synthesis: study of the promotion of Re on the reduction property of Co/Al_2O_3 catalysts by in situ EXAFS/XANES of Co K and Re LIII edges and XPS, Appl. Catal. A Gen. 264 (2004) 203–212, https://doi.org/10.1016/j.apcata.2003.12.049.

[52] M.P. Fernández-García, P. Gorria, M. Sevilla, A.B. Fuertes, R. Boada, J. Chaboy, G. Aquilanti, J.A. Blanco, Co nanoparticles inserted into a porous carbon amorphous matrix: the role of cooling field and temperature on the exchange bias effect, Phys. Chem. Chem. Phys. 13 (2011) 927–932, https://doi.org/10.1039/c0cp00396d.

[53] A.M.A. Saeedi, F.M. Gerriu, M. Ying, M.S. Alshammari, S.M. Heald, X. Li, H. J. Blythe, A.M. Fox, G.A. Gehring, Competing magnetic effects due to the incorporation of oxygen in thin films of (ZnCo)O, RSC Adv. 9 (2019) 38001–38010, https://doi.org/10.1039/c9ra06899f.

[54] S. Plzzini, K.J. Roberts, W.J. Phythian, C.A. English, G.N. Greaves, A fluorescence EXAFS study of the structure of copper-rich precipitates in Fe-Cu and Fe-Cu-Ni alloys, Philos. Mag. Lett. 61 (1990) 223–229, https://doi.org/10.1080/09500839008202362.

[55] A. Gaur, D. Shrivastava, K. Joshi, Copper K-edge XANES of Cu(I) and Cu(II) oxide mixtures, J. Phys. Conf. Ser. 190 (2009) 1–5, https://doi.org/10.1088/1742–6596/190/1/012084.

[56] M. Jiang, Y. Gao, Z. Wang, Z. Ding, Photocatalytic CO_2 reduction promoted by a $CuCo_2O_4$ cocatalyst with homogeneous and heterogeneous light harvesters, Appl. Catal. B Environ. 198 (2016) 180–188, https://doi.org/10.1016/j.apcatb.2016.05.055.

[57] S.H. Wu, D.H. Chen, Synthesis of high-concentration Cu nanoparticles in aqueous CTAB solutions, J. Colloid Interface Sci. 273 (2004) 165–169, https://doi.org/10.1016/j.jcis.2004.01.071.

[58] N. Weidler, S. Paulus, J. Schuch, J. Klett, S. Hoch, P. Stenner, A. Maljusch, J. Brötz, C. Wittich, B. Kaiser, W. Jaegermann, CoOx thin film deposited by CVD as efficient water oxidation catalyst: change of oxidation state in XPS and its correlation to electrochemical activity, Phys. Chem. Chem. Phys. 18 (2016) 10708–10718, https://doi.org/10.1039/c5cp05691h.

[59] L. Óvári, S. Krick Calderon, Y. Lykhach, J. Libuda, A. Erdohelyi, C. Papp, J. Kiss, H. P. Steinrück, Near ambient pressure XPS investigation of the interaction of ethanol with $Co/CeO_2(111)$, J. Catal. 307 (2013) 132–139, https://doi.org/10.1016/j.jcat.2013.07.015.

[60] M.C. Biesinger, B.P. Payne, A.P. Grosvenor, L.W.M. Lau, A.R. Gerson, R.S.C. Smart, Resolving surface chemical states in XPS analysis of first row transition metals, oxides and hydroxides: Cr, Mn, Fe, Co and Ni, Appl. Surf. Sci. 257 (2011) 2717–2730, https://doi.org/10.1016/j.apsusc.2010.10.051.

[61] R. Mutschler, E. Moioli, W. Luo, N. Gallandat, A. Züttel, CO_2 hydrogenation reaction over pristine Fe, Co, Ni, Cu and Al_2O_3 supported Ru: comparison and determination of the activation energies, J. Catal. 366 (2018) 139–149, https://doi.org/10.1016/j.jcat.2018.08.002.

[62] P. Summa, B. Samojeden, M. Motak, D. Wierzbicki, I. Alxneit, K. Świerczek, P. Da Costa, Investigation of Cu promotion effect on hydrotalcite-based nickel catalyst for CO_2 methanation, Catal. Today 384–386 (2022) 133–145, https://doi.org/10.1016/j.cattod.2021.05.004.

[63] H.-J. Freund, M.W. Roberts, Surface chemistry of carbon dioxide, Surf. Sci. Rep. 25 (1996) 225–273, https://doi.org/10.1016/S0167-5729(96)00007-6.

[64] J. Baltrusaitis, J. Schuttlefield, E. Zeitler, V.H. Grassian, Carbon dioxide adsorption on oxide nanoparticle surfaces, Chem. Eng. J. 170 (2011) 471–481, https://doi.org/10.1016/j.cej.2010.12.041.

[65] Y. Guo, S. Mei, K. Yuan, D.J. Wang, H.C. Liu, C.H. Yan, Y.W. Zhang, Low-temperature CO_2 methanation over CeO_2-supported Ru single atoms, nanoclusters, and nanoparticles competitively tuned by strong metal-support interactions and H-spillover effect, ACS Catal. 8 (2018) 6203–6215, https://doi.org/10.1021/acscatal.7b04469.

[66] Y. Li, Y. Men, S. Liu, J. Wang, K. Wang, Y. Tang, W. An, X. Pan, L. Li, Remarkably efficient and stable Ni/Y_2O_3 catalysts for CO_2 methanation: effect of citric acid addition, Appl. Catal. B Environ. 293 (2021), 120206, https://doi.org/10.1016/j.apcatb.2021.120206.

[67] K. Wang, Y. Men, S. Liu, J. Wang, Y. Li, Y. Tang, Z. Li, W. An, X. Pan, L. Li, Decoupling the size and support/metal loadings effect of Ni/SiO_2 catalysts for CO_2 methanation, Fuel 304 (2021), 121388, https://doi.org/10.1016/j.fuel.2021.121388.

[68] S. Kattel, B. Yan, J.G. Chen, P. Liu, CO_2 hydrogenation on Pt, Pt/SiO_2 and Pt/TiO_2: importance of synergy between Pt and oxide support, J. Catal. 343 (2016) 115–126, https://doi.org/10.1016/j.jcat.2015.12.019.

[69] W. Chen, B. Zijlstra, I.A.W. Filot, R. Pestman, E.J.M. Hensen, Mechanism of carbon monoxide dissociation on a cobalt Fischer–Tropsch catalyst, ChemCatChem 10 (2018) 136–140, https://doi.org/10.1002/cctc.201701203.